

Breakup of liquid jets: Thermodynamic perspectives

Fei Wang^{1,5,*}, Oleg Tschukin¹, Thomas Leisner^{3,4}, Haodong Zhang^{1,5}, and Britta Nestler^{1,2,5}

¹*Institute of Applied Materials, Karlsruhe Institute of Technology (KIT),
Straße am Forum 7, 76131 Karlsruhe, Germany*

²*Institute of Digital Materials Science, Karlsruhe University of Applied Sciences, Moltkestraße 30, 76133 Karlsruhe, Germany*

³*Institute of Environmental Physics, University of Heidelberg,
Im Neuenheimer Feld 229, 69120 Heidelberg, Germany*

⁴*Institute of Meteorology and Climate Research, Karlsruhe Institute of Technology (KIT),
Hermann-von-Helmholtz-Platz 1, 76344 Eggenstein-Leopoldshafen, Germany and*

⁵*Institute of Nanotechnology, Karlsruhe Institute of Technology (KIT),
Hermann-von-Helmholtz-Platz 1, 76344 Eggenstein-Leopoldshafen, Germany*

(Dated: February 14, 2024)

Breakup of a liquid jet into a chain of droplets is common in nature and industry. Previous researchers developed profound mathematic and fluid dynamic models to address this breakup phenomenon starting from tiny perturbations. However, the morphological evolution of the jets at large amplitude perturbations is still an open question. Here, we report a concise thermodynamic model based on the surface area minimization principle. Our results demonstrate a reversible breakup transition from a continuous jet via droplets towards a uniform-radius cylinder, which has not been found previously, but is observed in our simulations. This new observation is attributed to a geometric constraint, which was often overlooked in former studies. We anticipate our model to be a shortcut to tackle many similar highly nonlinear morphological evolutions without solving abstruse fluid dynamic equations for inviscid fluids.

As shown in Fig. 1(a), when we turn on a water-tap, a water jet trickles down and eventually breaks apart into a chain of droplets, which is also observed in the falling rain. This breakup phenomenon has drawn broad interests both in fundamental researches [1, 2, 6–14] and practical applications [3, 15–18]. In the 19th century, Joseph Plateau and Lord Rayleigh [4, 5] proposed a quintessential theory for droplet-formation considering tiny perturbations. However, the prevalence of large fluctuations in nature impedes the adaptability of this tenet. Hence, finding a satisfactory answer to the classic Plateau-Rayleigh question holds great promise not only for explicating a vast amount of unexplainable experiments [19] but also to guide and improve advanced technical applications.

Here, we report a concise mathematical-physical model to address the formation of droplets via the breakup of a liquid jet from a thermodynamic point of view. Traditionally, the Plateau-Rayleigh question was tackled by solving intricate fluid dynamic equations [20, 21]. Ipso facto, the occurrence of several irregular breakup phenomena via the phase-field model (Fig. 1(d)-ii, 1(e)-ii and 1(e)-iii) sheds light on the ambiguity of those conventional treatments. Presently, rather than pondering Navier-Stokes equations, we tackle the classic Plateau-Rayleigh question by considering the temporal dissipation of the Gibbs free energy of the system.

Our consideration is based on the thermodynamic principle of surface area minimizing with time irrespective of kinetics. Most importantly, one crucial fact is always overlooked that the initially cosinusoidal jet is getting disordered gradually with time, in lieu of remaining harmonic [22, 23]. Hence, we employ the following Fourier

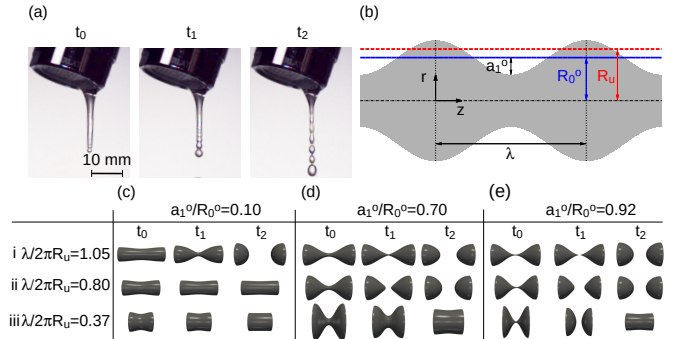


FIG. 1. Morphological evolution of liquid jets. (a) Formation of droplets when water trickles down from a water-tap. (b) 2D projection of a perturbed jet whose surface follows $r_o = R_0^0 + a_1^0 \cos(2\pi z/\lambda)$, where a_1^0 and λ are the amplitude and the wavelength of the initial harmonic perturbation, respectively. The volume of the jet is $\int_0^\lambda \pi r_o^2 dz = \pi[(R_0^0)^2 + \frac{1}{2}(a_1^0)^2]\lambda$ and we define $R_u^2 = (R_0^0)^2 + \frac{1}{2}(a_1^0)^2$ as the mean radius of the jet. (c), (d), (e), Morphological evolution of jets with different amplitudes and wavelengths via phase-field simulations. All the results in (c) (tiny perturbations) coincide with Rayleigh's theory [5]. Conversely, in (d)-ii, the breakup wavelength deviates from Rayleigh's prediction and this deviation also appears in (e)-ii. In (e)-iii, we observe an unusual breakup: a perturbed jet \rightarrow dispersed droplets \rightarrow continuous cylinder.

series [13]

$$r(t, z) = R_0(t) + \sum_{n=1}^K a_n(t) \cos nkz,$$

to depict the instantaneously changing jet-surface more precisely prior to the breakup with the initial condition: $a_1(t=0) = a_1^0$, $a_n(t=0) = 0$, $n \geq 2$ and $R_0(t=0) = R_0^0$.

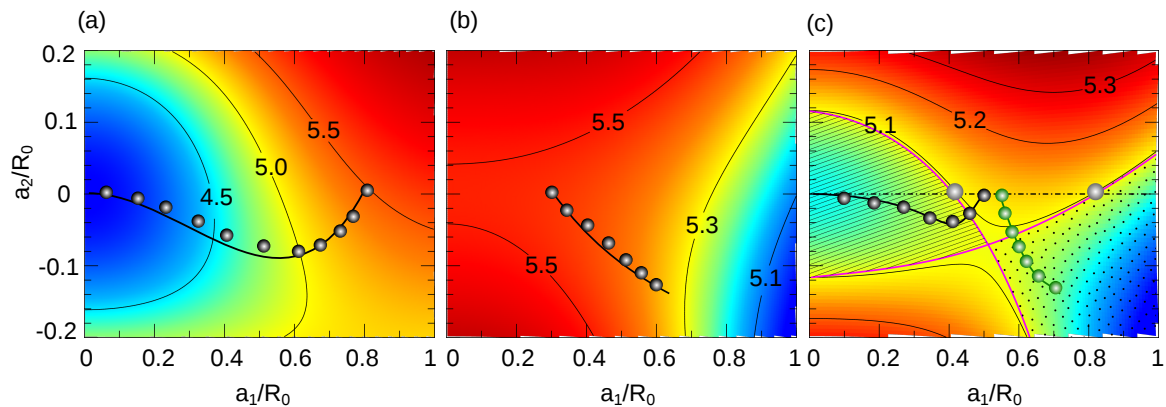


FIG. 2. **Surface area landscape.** (a), (b), (c), Surface area of jets as function of all the possible values of the first two Fourier coefficients (a_1/R_0 and a_2/R_0) with normalized wavelengths $\lambda/(2\pi R_u) = 0.37$ (Fig. 1iii), 1.05 (Fig. 1i), 0.80 (Fig. 1ii), respectively. The black/green circles denote the evolution routes of a_1/R_0 and a_2/R_0 from the phase-field simulations. The black/green dashed curves represent the evolution paths from the gradient descent method. The gray circles in (c) embrace a barrier interval along the horizontal dot-dashed line $a_2/R_0 = 0$. The hatched and dotted regions in (c) are partitioned by the isolines (magenta lines) of the saddle point of the surface area landscape.

0) = R_0^o . Here, $k = 2\pi/\lambda$ is the wavenumber, a_n are the Fourier coefficients, and K is the dimension of the Fourier series. It is noteworthy that the Fourier coefficients $a_n(t)$ are constrained by the volume conservation as $V(t) = \pi R_u^2 \lambda$, which yields $R_u^2 = R_0^2(t) + \frac{1}{2} \sum_{n=1}^K a_n^2(t)$, $\forall t$. The surface area of the jet is calculated by the following integral (see details in Refs. [13, 14])

$$S(a_1(t), a_2(t), \dots) = 2\pi \int_0^\lambda r(t, z) \sqrt{1 + [\partial_z r(t, z)]^2} dz.$$

For a given wavelength λ , we visualize the surface area landscape $S(a_1, a_2)$ for all possible values of the two Fourier coefficients a_1 and a_2 . Three typical surface area landscapes S as a function of a_1 and a_2 are illustrated in Fig. 2(a), (b) and (c) for short, long, and medium wavelengths, respectively. For the short (long) wavelength, the global minimum of the surface area is at $a_1 = 0$ (nearby the maximal value of a_1), so that the end-state is a uniform-radius cylinder (droplets). Interestingly, for the intermediate wavelength (Fig. 2(c)), two local minima locate inside the hatched and the dotted regions, which correspond to a final state of a uniform-radius cylinder and a droplet-structure, respectively. The domain outside these two regions, which is called as barrier zone, highlights initial configurations whose surface area is greater than the ones in the hatched and dotted regions and can evolve either into a uniform-radius cylinder or into droplets. As aforementioned, we consider the evolution of a jet with a cosinusoidal perturbation with $a_2^o = 0$ at the beginning. This initial setup corresponds to the horizontal dot-dashed line in Fig. 2(c) and overlaps the barrier zone between the two gray circles embracing a barrier interval. The critical configuration for the droplet-formation buries inside this barrier interval, which is also obtained for many other medium

wavelengths. Those barrier intervals versus wavelengths is represented by the shaded region in Fig. 3(a). Left below and right above this shaded region, the jet has a surface area landscape as in Fig. 2(a) and 2(b), respectively.

Next, we adopt the phase-field simulations [24–27] and the gradient descent method (GDM) [28] to scrutinize the evolution kinetics and the critical breakup configuration. In the phase-field model, a phase order parameter φ is introduced to characterize the phase state. For instance, $\phi = 1$ denotes the jet, $\phi = 0$ represents the surrounding, and ϕ continuously varies from 1 to 0 in the diffuse interface from the jet to the surrounding. The evolution of the phase order parameter $\partial_t \varphi$ is such as to reduce the Ginzburg-Landau energy functional, $\mathcal{S}(\varphi)$, following GDM as

$$\partial_t \varphi = -\delta \mathcal{S} / \delta \varphi - \mathcal{L}.$$

Here, \mathcal{L} is a Lagrange multiplier to ensure the volume conservation. The Ginzburg-Landau energy functional is expressed as [29] $\mathcal{S}(\varphi) = \int_\Omega [\kappa (\nabla \varphi)^2 + \omega(\varphi)] d\Omega$, where κ is the gradient energy coefficient and $\omega(\varphi)$ denotes an obstacle potential energy (see supplemental document for details).

Since surface tension is a joint effect of adhesion and cohesion, which both are conservative forces, the evolution direction of the Fourier coefficients follows the gradient of the surface area $-(\partial_{a_n} S) \in \mathbb{R}^K$, namely,

$$\partial_t a_n = -\partial_{a_n} S.$$

The time evolution is subjected to the aforementioned initial condition. In Fig. 2(a) and 2(b), the black solid lines depict the kinetic routes along the steepest gradient for two initial setups $a_1^o/R_0^o = 0.8$ and 0.3, respectively. The GDM paths are well consistent with the

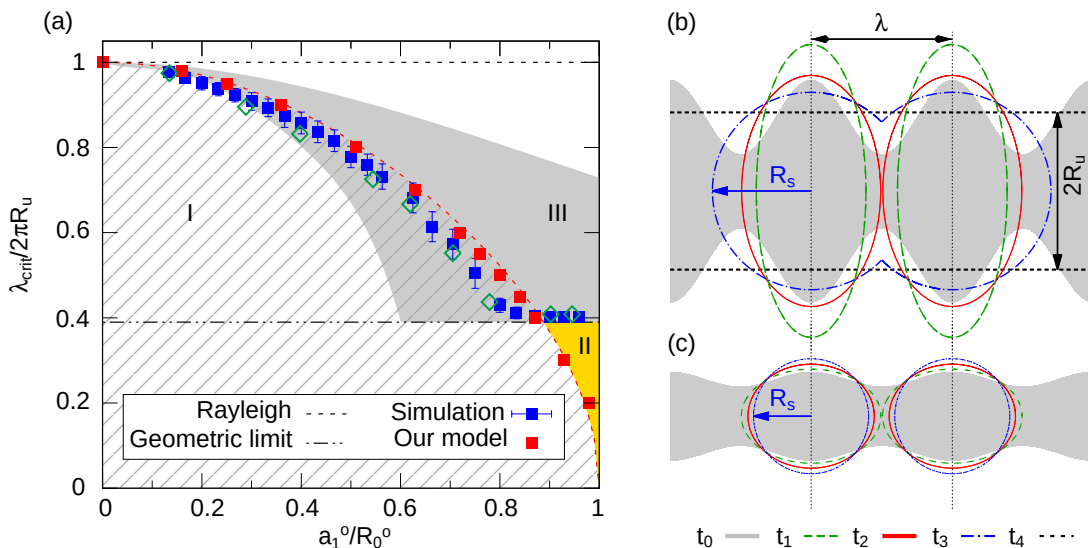


FIG. 3. **Stability diagram.** (a) The normalized critical breakup wavelength $\lambda_{\text{crit}}/(2\pi R_u)$ as a function of the scaled initial amplitude a_1^o/R_0^o . The red and blue squares depict the results from the gradient descent method and the Allen-Cahn model, respectively. The red dashed line is the fitting curve for the red squares. The green diamonds demonstrate the simulation results from a fluid dynamics model (see supplemental document), which are in good agreement with our model. The dot-dashed line denotes the geometric criterion. The gray shaded region illustrates all the barrier intervals shown in Fig. 2(c) for different wavelengths. (b) A reversible separation in II from a continuous jet via separated ellipsoid-shaped droplets towards a uniform-radius cylinder. (c) Regular breakup in III, where R_s is the radius of the resulting spheroids.

simulation results (black circles), which are achieved by applying the Fourier transformation to the jet-surface to obtain the Fourier coefficients at different time steps of the simulation. In Fig. 2(c), the black and green lines (GDM)/circles (simulations) illustrate the evolution paths of two exemplary setups inside the barrier interval, $a_1^o/R_0^o = 0.48$ and 0.55 , which transform into a uniform-radius cylinder and a droplet-structure, respectively. By using binary search algorithm for initial setups inside the barrier interval, the critical breakup configurations are identified by GDM and simulations, as depicted by the red and blue squares, respectively, in Fig. 3(a).

As shown in Fig. 3(a), our simulation results coincide quite well with GDM when $a_1^o/R_0^o \lesssim 0.88$. While $a_1^o/R_0^o > 0.88$, the simulation results become a horizontal line which surprisingly deviates from GDM. A heedful scrutiny on those unusual simulations reveals that the jet indeed firstly breaks apart into several oval-shaped droplets (see Fig. 1(e)-iii, t_1) in accordance with GDM. However, afterwards, the spheroidization of the oval droplets rebuilds contact between neighbors and finally leads to a uniform-radius cylinder. This process is sketched in Fig. 3(b) and decided by a geometric limit where the distance between the centroids of the resulting spheroids $2R_s$ is equal to the wavelength of the perturbation. With the volume conservation condition $\frac{4}{3}\pi R_s^3 = \pi R_u^2 \lambda$, the geometric criterion is derived: $\lambda_{\text{crit}} = \sqrt{6}R_u$, which is shown by the horizontal dot-dashed line in Fig. 3(a) and provides a reasonable interpretation for those abnormal simulative morphological

evolutions deviating from GDM.

As a result of the geometric constraint, the stability diagram in Fig. 3(a) is divided into three regimes: I (hatched line), II (orange) and III (excluding I and II). In I, the perturbed jet directly evolves into a uniform-radius cylinder. In II, the jet firstly transforms into separated prolate spheroids, elongated in the radial dimension, as shown by the green line in Fig. 3(b). Afterwards, spheroidization rebuilds a chain of connected droplets (red and blue lines), which eventually evolves into a uniform-radius cylinder (black dashed line). In III, the jet also decomposes into ellipsoid-shaped droplets, which are, however, oblate this time. As schematically shown in Fig. 3(c), the decrease in the surface area of the oblate spheroids results in an augmentation of the gap spacing between adjacent droplets. The demarcation between II and III is defined by the locus that neither prolate nor oblate, but spherical droplets are precisely tangent to their neighbors. This critical configuration is actually the geometric limit mentioned above.

In conclusion, we have proposed a thermodynamic concept to address the classic Plateau-Rayleigh question. The surface area landscape method combining with the gradient descent approach as well as the geometric constraint enables us to reveal a transient reversible breakup phenomenon. Furthermore, precise knowledge of non-linear stability analysis for large perturbations is still lacking at present, which makes it difficult to gain efficient predictions for highly non-linear morphological evolutions. We anticipate that the surface area landscape

method proposed in the present work is an alternative for nonlinear stability analysis to see through more physical phenomena.

Acknowledgments: The authors thank for support through the coordinated program Virtual Materials Design (VirtMat) within the Helmholtz association and through the Gottfried-Wilhelm Leibniz programme NE 822/31. F.W. is grateful to the discussion with W. C. Carter (MIT). F.W. designed the phase-field simulations. F.W. and O.T. contributed to the concept of the surface area landscape. F.W. and H.Z. discussed the gradient descent method and wrote the first draft of the manuscript. T.L. contributed to the picture illustrating the breakup of a liquid jet under water tap. T.L. and B.N. interpreted the thermodynamic concept and revised the manuscript. All authors contributed to the manuscript preparation.

* fei.wang@kit.edu

- [1] J. J. Kaufman *et al.*, Structured spheres generated by an in-fibre fluid instability, *Nature* **487**, 463 (2012).
- [2] A. Passian and T. Thundat, Materials science: The abilities of instabilities, *Nature* **487**, 440 (2012).
- [3] H. Wijshoff, The dynamics of the piezo inkjet printhead operation, *Phys. Rep.* **491**, 77 (2010).
- [4] L. Rayleigh, On the instability of jets, *Proc. Math. Soc.* **10**, 4 (1878).
- [5] L. Rayleigh, On the capillary phenomena of jets, *Proc. Math. Soc.* **29**, 196 (1879).
- [6] J. R. Royer *et al.*, High-speed tracking of rupture and clustering in freely falling granular streams, *Nature* **459**, 1110 (2009).
- [7] I. G. Loscertales *et al.*, Micro/nano encapsulation via electrified coaxial liquid jets, *Science* **295**, 1695 (2002).
- [8] M. Moseler and U. Landman, Formation, stability, and breakup of nanojets, *Science* **289**, 1165 (2000).
- [9] A. S. Utada, E. L. Lorenceau, D. R. Link, P. D. Kaplan, H. A. Stone, and D. A. Weitz, Monodisperse double emulsions generated from a microcapillary device, *Science* **308**, 537 (2005).
- [10] S. Haefner *et al.*, Influence of slip on the Plateau-Rayleigh instability on a fibre, *Nat. Commun.* **6**, 7409 (2015).
- [11] V. Cardoso and O. J. C. Dias, Rayleigh-Plateau and Gregory-Laflamme instabilities of black strings, *Phys. Rev. Lett.* **96**, 181601 (2006).
- [12] G. Prado, Y. Amarouchene, and H. Kellay, Experimental evidence of a Rayleigh-Plateau instability in free falling granular jets, *Phys. Rev. Lett.* **106**, 198001 (2011).
- [13] F. Wang, O. Tschukin, T. Leisner, H. Zhang, B. Nestler, M. Selzer, G.C. Marques, J. Aghassi-Hagmann, *Acta Mater.* **192**, 20–29 (2020).
- [14] F. Wang and B. Nestler, *Scr. Mater.* **113**, 167–170 (2016).
- [15] P. P. Bhat *et al.*, Formation of beads-on-a-string structures during break-up of viscoelastic filaments, *Nat. Phys.* **6**, 625 (2010).
- [16] E. C. Garnett *et al.*, Self-limited plasmonic welding of silver nanowire junctions, *Nat. Mater.* **11**, 241 (2012).
- [17] R. W. Day *et al.*, Plateau-Rayleigh crystal growth of periodic shells on one-dimensional substrates, *Nat. Nanotechnol.* **10**, 345 (2015).
- [18] Z. Xue *et al.*, Engineering island-chain silicon nanowires via a droplet mediated Plateau-Rayleigh transformation, *Nat. Commun.* **7**, 12836 (2016).
- [19] A. V. Boukharov *et al.*, Dynamics of cryogenic jets: non-Rayleigh breakup and onset of nonaxisymmetric motions, *Phys. Rev. Lett.* **100**, 174505 (2008).
- [20] M.-C. Yuen, Non-linear capillary instability of a liquid jet, *J. Fluid Mech.* **33**, 151 (1968).
- [21] A. H. Nayfeh, Nonlinear stability of a liquid jet, *Phys. Fluids* **13**, 841 (1970).
- [22] W. C. Carter and A. M. Glaeser, The effect of finite amplitude perturbations on the stability of continuous phases, *Mater. Sci. Eng.* **89**, 41 (1987).
- [23] F. A. Nichols and W. W. Mullins, Surface- (interface-) and volume-diffusion contributions to morphological changes driven by capillarity, *Trans. Metall. Soc. AIME* **233**, 1840–1848 (1965).
- [24] F. Wang, P. Altschuh, A.M. Matz, J. Heimann, B.S. Matz, B. Nestler, and N. Jost, *Acta Mater.* **170**, 138–154 (2019).
- [25] P. Laxmipathy, F. Wang, M. Selzer, and B. Nestler, *Acta Mater.* **204**, 116497 (2021).
- [26] P. Laxmipathy, F. Wang, M. Selzer, and B. Nestler, *Comput. Mater. Sci.* **186**, 109964 (2021).
- [27] F. Wang, A. Choudhury, C. Strassacker, and B. Nestler, *J. Chem. Phys.* **137**, 034702 (2012).
- [28] Y. Wu, F. Wang, M. Selzer, and B. Nestler, *Phys. Rev. E* **100**, 041102 (2019).
- [29] J. W. Cahn and J. E. Hilliard, Free energy of a nonuniform system. I. Interfacial free energy, *J. Chem. Phys.* **28**, 258–267 (1958).